SLAC-PUB-9626
March 2003

The single-mode CSR instability of a bunched beam. *

S. Heifets
Stanford Linear Accelerator Center, Stanford University, Stanford, CA 94309, USA

Abstract

The coherent synchrotron radiation (CSR) instability at the shielding threshold may be driven by a single synchronous mode excited by the beam in the beam pipe. The instability in this case has been analyzed [1] in the coasting beam approximation neglecting synchrotron motion. The later becomes important at large time intervals in storage rings where it substantially affects the beam dynamics. The single-mode CSR instability of a bunched beam with the synchrotron motion taken into account is described in this paper both in linear and nonlinear regimes. Analysis is relevant to other instabilities where the interaction is dominated by a single mode.

Introduction

The coherent synchrotron radiation (CSR) can drive beam instability. In the previous paper [1] we studied the CSR instability [2] of a coasting beam interacting with a single wave-guide mode. The argument for using the coasting beam model aside of substantial simplification of the theory was based on the fact that the wave length of the relevant perturbation is small compared to the bunch length. The instability was studied both in the linear and non-linear regimes. It was shown that even on the large time scale comparable or larger than the damping time there is no saturation of the instability: the amplitude of the perturbation keeps growing slowly but steadily.

To be valid on such time intervals, however, the approach has to be reconsidered taking into account the synchrotron motion. Another motivation for the study is provided by the recent proposal to build a dedicated storage ring for generation of the infrared coherent radiation [3].

*Work supported by Department of Energy contract DE–AC03–76SF00515.

The paper is organized in the following way. First, the basic equations describing the beam dynamics and the interaction of the beam with the excited EM wave are obtained. Then, it is shown that although the steady-state solution exists, it is unstable and the growth rate for a bunched beam is determined in the linear approximation. For existing machines, the linear regime is limited to the time intervals less than a microsecond. Therefore, it is important to consider the nonlinear regime of the instability. The qualitative analysis of the nonlinear regime and the estimate of the growth rate is given in the following two sections. Then, the results of numeric simulations are presented and compared with the qualitative analysis.

Basic equations

The beam dynamics is described neglecting the nonlinearity of the rf field assuming that the nonlinearity is dominated by the beam-wave interaction $V_B(z,t)$,

$$\frac{dz}{dt} = -\eta c\delta, \quad \frac{d\delta}{dt} = \frac{\omega_s^2}{\eta c}\, z + V_B(z,t), \tag{1}$$

where z is position of a particle along the bunch, δ is the relative energy offset, $\omega_s/(2\pi)$ is the synchrotron frequency, and η is the momentum compaction factor. The EM wave excited by the beam in the wave guide is defined by the wave frequency ω_w, the wave vector $q_w = \omega_w/c$, the loss factor per unit length χ, and the group velocity β_g. V_B is defined [1] by the distribution function f, $\int dzd\delta f(z,\delta,t) = 1$ (see Appendix)

$$V_B(z,t) = -\frac{r_e N_B c^2}{\gamma}(1-\beta_g)\chi \int_{-\infty}^{t} dt' d\delta' f[z+c(t-t')(1-\beta_g), \delta', t'] e^{-i(1-\beta_g)\omega_w(t-t')} + c.c. \tag{2}$$

Here N_B is the number of particles per bunch, and γ is the relativistic parameter of the beam (not to be confused with the radiation damping $\gamma_{SR} = 1/\tau_{SR}$ below).

It is convenient to use dimensionless variables (τ, ζ, P), and interaction $V(\zeta,\tau)$ introducing

$$\tau = \mu t, \quad \zeta = q_w z, \quad P = -\frac{\eta\omega_w}{\mu}\delta, \quad V(\zeta,\tau_B) = \frac{\eta\omega_W}{\mu^2}\, V_B(z,t), \tag{3}$$

where μ depends on the peak density in a bunch $n_B = N_B/(\sigma_B\sqrt{2\pi})$.

$$(\frac{\mu}{c})^3 = \frac{r_e n_B}{c\gamma}(1-\beta_g)\chi\eta\omega_w. \tag{4}$$

It is convenient to use notations

$$\kappa = (\frac{\omega_w}{\mu})(1-\beta_g), \quad \Delta = \frac{\eta\omega_w\delta_0}{\mu}, \quad \Gamma = \frac{\gamma_{SR}}{\mu}, \quad \Omega = \frac{\omega_s}{\mu}, \tag{5}$$

where δ_0 is the rms of the relative energy spread. The corresponding Hamiltonian H is

$$H(\zeta,P,\tau) = \frac{P^2}{2} + \frac{\Omega^2\zeta^2}{2} + U(\zeta,\tau). \tag{6}$$

The potential U is defined by $dU/d\zeta = V$,

$$V(\zeta, \tau_B) = -\lambda^3 \int_{-\infty}^{\tau} d\tau' dP' F[\zeta + (\tau - \tau')\kappa, P', \tau'] e^{-i\kappa(\tau-\tau')} + c.c. \tag{7}$$

where

$$\lambda^3 = \sqrt{2\pi}\frac{\Delta}{\Omega}, \tag{8}$$

and the integration over τ' from $-\infty$ implies that a small $\epsilon- > +0$ is added to the exponent.

The distribution function $F(\zeta, P, \tau)$ is normalized, $\int dP d\zeta F(\zeta, P, \tau) = 1$ and satisfies the Fokker-Plank equation

$$\frac{\partial F}{\partial \tau} + P\frac{\partial F}{\partial \zeta} - [\Omega^2\zeta + V(\zeta, \tau)]\frac{\partial F}{\partial P} = \Gamma \frac{\partial}{\partial P}[\Delta^2 \frac{\partial F}{\partial P} + P\, F]. \tag{9}$$

Let us define $w(\zeta, \tau)$, $V(\zeta, \tau) = w(\zeta, \tau) + c.c.$. The Fourier harmonics $\tilde{w}(q, \tau)$

$$w(\zeta, \tau) = \int \frac{dq}{2\pi} \tilde{w}(q, \tau) e^{iq\zeta} \tag{10}$$

is related to F,

$$\frac{\partial \tilde{w}(q, \tau)}{\partial \tau} = i(q-1)\,\kappa\,\tilde{w}(q, \tau) - \lambda^3 \int d\zeta\, dP e^{-iq\zeta} F(\zeta, P, \tau). \tag{11}$$

Note that $\Delta/\Omega = q_w \sigma_B >> 1$ for the high frequency waves with the wave length $2\pi/q_w$ which is small in comparison to the rms bunch length σ_B.

Parameters of four typical machines are given in Table.

Table 1: **Parameters for several machines.**

	LER	HER	ALS	VUV NSLS
μ, $1/\mu s$	8.15	31.9	22.7	2.7
κ	138.9	98.5	138.4	121.3
Ω	3.9E-3	1.3E-3	0.33E-3	14.E-3
Δ	0.072	0.031	0.012	0.92

1 Steady-state solution

The Fokker-Plank Eq. (9) has a formal steady-state solution which, after integration over P, takes the form

$$F(\zeta) = \frac{1}{|N|} e^{-\frac{1}{\Delta^2}[\frac{\Omega^2\zeta^2}{2} + U(\zeta)]}, \tag{12}$$

where $|N|$ is normalization constant and $U(\infty) = 0$.

It can be solved by iterations starting with a Gaussian bunch

$$F_0(\zeta) = \frac{1}{\sqrt{2\pi\Delta^2}} e^{-\frac{1}{2}(\frac{\Omega\zeta}{\Delta})^2}. \tag{13}$$

In the first iteration, the potential and the distribution function are

$$\begin{aligned} U_1(\zeta) &= -\frac{2\lambda^3}{\kappa} \int_\zeta^\infty dz' F_0(z) \sin(z - z') \\ F_1(\zeta) &= \frac{1}{|N|\sqrt{2\pi\Delta^2}} e^{-\frac{1}{\Delta^2}[\frac{\Omega^2\zeta^2}{2} + U_1(\zeta)]}. \end{aligned} \tag{14}$$

The potential is given in terms of the error function

$$U_1(\zeta) = \mathrm{Re}\{\frac{2\Delta}{\kappa\Omega}\sqrt{\frac{\pi}{2}} e^{-\frac{\Delta^2}{2\Omega^2}} [e^{i\zeta}\, Erfi(\frac{\Delta^2 - i\Omega^2\zeta}{\sqrt{2}\Delta\Omega}) - \sin(\zeta)]\}. \tag{15}$$

The iterations can be repeated. The distribution functions F_0 and F_1 calculated with parameters $\Delta = 0.3$, $\Omega = 0.01$, $\kappa = 90$ are shown in Fig.(1). The difference is very small. However, the linear analysis below shows that such a steady-state solution is unstable.

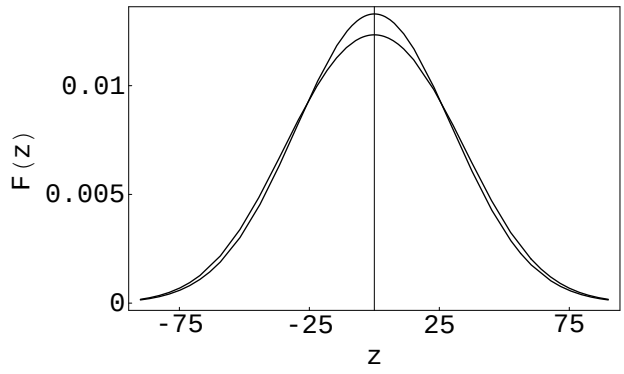

Figure 1: The steady-state solution obtained by iterations.

The analysis presented above leaves open question whether there is a time-independent solution $F(\zeta, \tau) = F(\zeta)$ with large amplitude of perturbation $V(\zeta)$.

The following arguments indicate (although do not prove) that such a solution does not exist.

Eq. (7) can be written as

$$\begin{aligned} V(\zeta) &= A(\zeta)\, e^{i\zeta} + c.c. \\ A(\zeta) &= -\frac{\lambda^3}{\kappa} \int_\zeta^\infty d\zeta' e^{-i\zeta'} F(\zeta'). \end{aligned} \tag{16}$$

Hence, the steady-state solution is given by the system of equations

$$\begin{aligned}
&\frac{dU(\zeta)}{d\zeta} = A(\zeta)e^{i\zeta} + c.c.,\\
&\frac{dA(\zeta)}{d\zeta} = \frac{\lambda^3}{\kappa}\, e^{-i\zeta}\, F(\zeta), \quad F(\zeta) = \frac{1}{|N|} e^{-\frac{1}{\Delta^2}[\frac{\Omega^2\zeta^2}{2}+U(\zeta)]},\\
&|N| = \int d\zeta e^{-\frac{1}{\Delta^2}[\frac{\Omega^2\zeta^2}{2}+U(\zeta)]}.
\end{aligned} \tag{17}$$

The system is suitable for simulations.

The trivial solution $A(\zeta) = (a/2)e^{-i\zeta}$, $U(\zeta) = Re[a]$ does not exists. Indeed, the second equation gives $a' - ia =$ realfunction. Hence, $a(\zeta) = 0$, while $a' \neq 0$.

It can be proven that a solution of the form

$$U(\zeta) = a\, \cos(\zeta - \zeta_0), \tag{18}$$

where a and ζ_0 are real functions with slow dependence on ζ does exist but with $a = const$. Such a solution can be obtained by direct numeric solution of Eq. (18). However, the obtained solution gives $U(\zeta)$ oscillating with a constant amplitude for all ζ what is not acceptable. This arguments show that the steady-state solution which is non-zero only behind the bunch, probably, does not exist.

2 Linerized Vlasov equation with the synchrotron motion

In this section, we show that the steady-state solution with the zero amplitude of the perturbation is unstable: a small perturbation grows in time exponentially.

With the synchrotron motion taken into account, there is no periodicity over ζ even for a bunch interacting with a single EM wave. Let us introduce the Fourier harmonics of the distribution function

$$F(\zeta, P, \tau) = \int \frac{dq}{2\pi} e^{iq\zeta} \tilde{F}(q, P, \tau). \tag{19}$$

Assuming the time dependence of the harmonics in the form $\tilde{w}(q,\tau) = \hat{w}(q)e^{-i\nu\tau}$, $\tilde{F}(q,P,\tau) = \hat{F}(q,P)e^{-i\nu\tau}$ with amplitudes $\hat{F}(q,P)$ and $\hat{w}(q)$, respectively, we get from Eq. (11):

$$\hat{w}(q) = -i\lambda^3 \frac{\int dP \hat{F}[q,P]}{(q-1)\kappa + \nu}. \tag{20}$$

In the zero approximation, the distribution function is $F_0(\zeta, P)$,

$$F_0(\zeta, P) = \frac{1}{Z} e^{-\frac{1}{\Delta^2}(\frac{P^2}{2}+\frac{\Omega^2\zeta^2}{2})}, \tag{21}$$

where the normalization constant $Z = 2\pi\Delta^2/\Omega$. The contribution of F_0 to Eq. (20) is exponentially small when $q \simeq 1$.

In the linear approximation, $F(\zeta, P, \tau) = F_0 + [f(\zeta, P)e^{-i\nu\tau} + c.c.]$, and $\hat{F}(q, P)$ in Eq. (20) can be replaced by $\hat{f}(q, P)$.

Eq. (9) is reduced to the Vlasov equation for $f(\zeta, P, \tau)$:

$$\frac{\partial f}{\partial \tau} + P\frac{\partial f}{\partial \zeta} - \Omega^2\zeta\,\frac{\partial f}{\partial P} = V(\zeta, \tau)\,\frac{\partial F_0}{\partial P}. \tag{22}$$

Eq. (22) can be easily solved using characteristics

$$\zeta(\tau) = \zeta_0\cos(\Omega\tau) + \frac{P_0}{\Omega}\sin(\Omega\tau), \quad P(\tau) = -\Omega\zeta_0\sin(\Omega\tau) + P_0\cos(\Omega\tau). \tag{23}$$

The solution is

$$f(\zeta, P, \tau) = -\frac{F_0(\zeta, P)}{\Delta^2}\int_{-\infty}^{\tau} d\tau'[\Omega\zeta\sin\phi + P\cos\phi]\,V[\zeta\cos\phi - \frac{P}{\Omega}\sin\phi, \tau'], \tag{24}$$

where $\phi = \Omega(\tau - \tau')$.

Substitute Eqs. (24) and (21) in the definition of the Fourier harmonics

$$\hat{f}(q, P) = \int d\zeta e^{-iq\zeta + i\nu\tau}\, f(\zeta, P, \tau). \tag{25}$$

Integration over P and ζ gives

$$\int dP\hat{f}(q, P) = \frac{iq}{\Omega}\int\frac{dq'}{2\pi}\hat{V}(q')e^{-\frac{1}{2}(\frac{\Delta}{\Omega})^2(q-q')^2}S(q, q'), \tag{26}$$

where

$$S(q, q') = \int_0^\infty d\tau e^{i\nu\tau}\sin(\Omega\tau)e^{-(\frac{\Delta}{\Omega})^2 q\,q'\,[1-\cos(\Omega\tau)]}. \tag{27}$$

Combining Eqs. (20), (26) we get

$$\hat{V}(q) = \frac{\lambda^3\,q}{\Omega[\nu + (q-1)\kappa]}\int\frac{dq'}{2\pi}\hat{V}(q')e^{-\frac{1}{2}(\frac{\Delta}{\Omega})^2(q-q')^2}S(q, q'). \tag{28}$$

As it was mentioned above, the ratio $\Omega/\Delta = 1/(q_w\sigma_b) << 1$ for the short wave length perturbations. Therefore, the integral in Eq. (28) can be estimated taking factors $\hat{V}(q')S(q, q')$ at $q' = q$. Eq. (28) then gives the dispersion equation

$$1 = \frac{\lambda^3 q}{\Delta\sqrt{2\pi}}\,\frac{S(q, q)}{\nu + (q-1)\kappa}. \tag{29}$$

The function $\Omega\,S(q, q)$ is function of two parameters

$$S(q, q) = \frac{1}{\Omega}\int_0^\infty dx\sin(x)e^{i(\nu/\Omega)x}e^{-b^2(1-\cos x)}, \tag{30}$$

where $b = q\Delta/\Omega >> 1$. The main contribution to the integral Eq. (30) is given by $|x| << 1$. The other contributions come from the narrow vicinities of $x_k = 2\pi k$, k = integer, which cancel each other provided there are no resonances ν/Ω = integer. Therefore, for $\Omega/\Delta << 1$, the integral can be simplified,

$$S(q,q) = \frac{\Omega}{(q\Delta)^2} G[\frac{\nu}{q\Delta}], \tag{31}$$

where

$$G[a] = \int_0^\infty x dx e^{iax} e^{-x^2/2}. \tag{32}$$

For large $|a| >> 1$, $G(a) \simeq -(1/a^2)$, and Eq. (29) gives

$$\nu^2[\nu + (q-1)\kappa] = -\frac{\lambda^3 q}{\sqrt{2\pi}} \frac{\Omega}{\Delta}. \tag{33}$$

Using definition Eq. (8), we get for $q = 1$

$$\nu^3 = -\frac{\lambda^3 \Omega}{\Delta\sqrt{2\pi}} = -1. \tag{34}$$

The growth rate $Im(\nu) = \sin[\pi/3]$ exactly corresponds to the growth rate defined before [1] for a cold beam (i.e. for $\Delta << \nu$). The synchrotron motion does not change the result provided $\Omega/\Delta << 1$, i.e. for the short wave lengths.

The value $q = 1$ corresponds to the modulation $V(\zeta,\tau) \propto e^{i(\zeta - \nu\tau)}$ and the perturbation of the distribution function of the form $F(\zeta, P, \tau) \propto e^{i\zeta} = e^{iq_w z}$, i.e. the spatial modulation with the wave length of the EM wave.

For $q \neq 1$, the growth rate is reduced provided $\kappa >> 1$. The function $Im[\nu]$ is shown in Fig. (2) as function of q for $\kappa = 25$.

Eq. (33) gives for $1 >> |q-1|\kappa >> |\nu|/\kappa$

$$\nu^2 = -\frac{1}{(q-1)\kappa}. \tag{35}$$

Eq. (35) gives the estimate for the width of the resonance and shows that instability is substantial only for harmonics of the distribution function $F(q)$ in the narrow vicinity of $q = 1$. From these results, it is clear that, in the linear approximation, different EM modes in the beam pipe can be considered independently.

3 Particle motion in the nonlinear regime: qualitative analysis

Fast initial growth predicted by the linear theory is limited to a short period of time of the order of the inverse growth rate, $\tau \simeq 1$, $t \simeq 1/\mu$. After that, the growth of the amplitude is substantially nonlinear. For the time intervals small compared with the

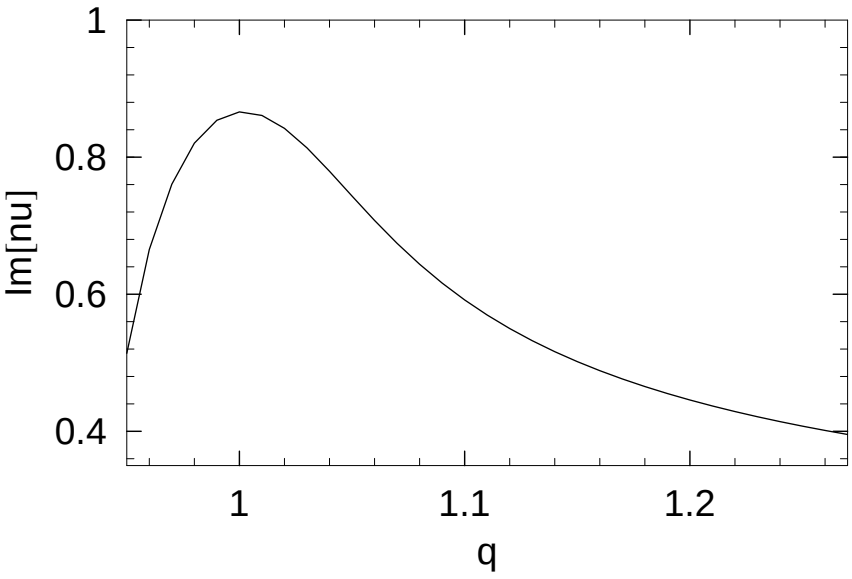

Figure 2: The growth rate $Im[\nu]$ as function of the detuning for $\kappa = 25$.

period of synchrotron oscillations, the nonlinear beam dynamics is the same as for the case of a coasting beam [1]. Describing the non-linear behavior at larger time we found that it is necessary to distinguish the short-range and the long-range nonlinear regimes. The first regime can be analyzed similarly to the analysis given for the coasting beam [1] and is presented in this section. In spite of similarity, the growth rate in this regime is quite different from the one for coasting beam and depends on Ω. Analysis and simulations of the second regime are given in the following sections.

As it shown above, in the linear regime the beam-wave interaction with a single mode can be written as $V(\zeta,\tau) = aq_0 \sin(q_0\zeta - \nu\tau)$ with the wave vector $q_0 \simeq 1$ and the amplitude a exponentially growing in time. We assume that in the nonlinear regime $V(\zeta,\tau)$ has the same form where the mode frequency $\nu(\tau)$ and the amplitude $a(\tau)$ are real but the amplitude a and the tune ν may vary slowly in time.

Interaction with such a mode can be described by the system of equations equivalent to the Fokker-Plank equation Eq. (9),

$$\dot{\zeta}(\tau) = P, \quad \dot{P}(\tau) + \Omega^2\zeta = -\Gamma P - a\, q_0\, \sin(q_0\zeta - \nu\tau). \tag{36}$$

The quantum fluctuations can be taken into account by adding a random force to the right-hand-side of the second equation but can be neglected for a time intervals smaller than the damping time.

The left-hand-side of Eq. (36) corresponds to motion of a particle in the potential, see Fig. (3),

$$U(\zeta,\tau) = \frac{\Omega^2\zeta^2}{2} + a[1-\cos(q_0\zeta - \nu\tau)]. \tag{37}$$

The potential has minima at the points defined by the equation

$$\zeta + \frac{q_0 a}{\Omega^2}\sin(q_0\zeta - \nu\tau) = 0. \tag{38}$$

The potential is a chain of micro-potential wells. For $a >> \Omega^2$, they are centered at

$$\zeta_k(\tau) \simeq \frac{1}{q_0}(1 - \frac{\Omega^2}{\omega^2})(\nu\tau + 2\pi k), \quad k = \text{integer}, \tag{39}$$

where $\omega^2 = \Omega^2 + q_0^2\, a$. Eq. (39) is valid for $(\Omega/\omega)^2|\nu\tau + 2\pi k)| < 1$.

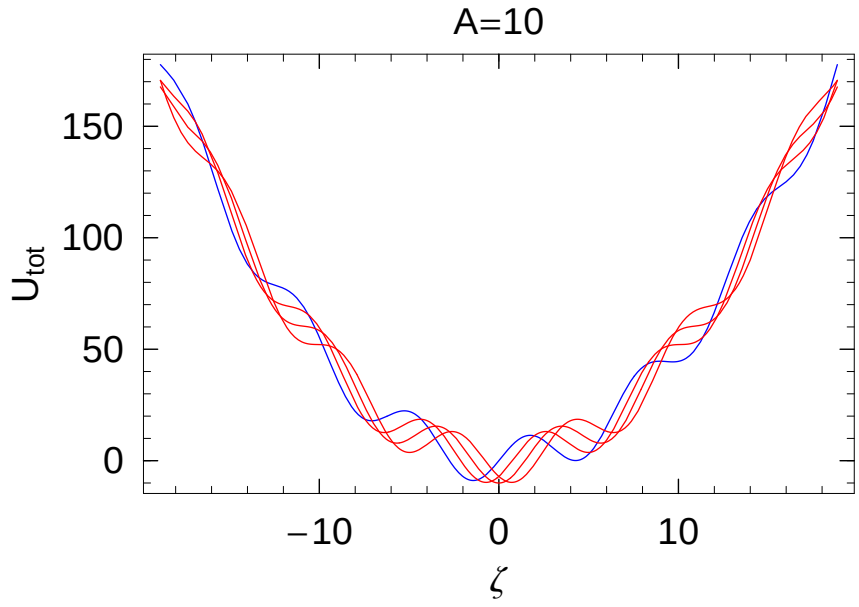

Figure 3: The total potential $U_{tot} = \zeta^2/2 + a\sin(\zeta - \nu\tau)$ for $\nu\tau = (0, \pi/4, \pi/2, 3\pi/4)$ and $a = 10$. A particle trapped in the local minimum remains trapped and moves with the minimum until it reaches large $\zeta \simeq a$.

For a fixed τ and large $a >> 1$, there are approximately

$$n_{well} \simeq \frac{a\, q_0^2}{\pi\Omega^2} \tag{40}$$

potential wells within the distances $|\zeta| < a$ separated by $\Delta\zeta = 2\pi/q_0$, see Fig. (3).

In the linear approximation, the wave amplitude $a(\tau)$ grows to $a \simeq 1$ much faster than the synchrotron period. Hence, initially, position and momentum of a particle do not

change. Particles remain distributed approximately uniformly in the phase space within $|\zeta| < \Delta/\Omega$ and $|P| < \sqrt{2\Delta}$.

Then, trapped particles start synchrotron oscillations with the amplitude $z_{max} < \pi$. The frequency of small oscillations is

$$\omega = \sqrt{a + \Omega^2} \tag{41}$$

and the maximum momentum of a trapped particle is of the order of $P_{max} = z_{max}\omega$. Note that the frequency of oscillations of a trapped particle ω may be large compared to the synchrotron frequency Ω for amplitudes $a >> 1$.

The depth of the potential wells is proportional to the amplitude a. The energy of a particle $H = \omega J$ where action $J = const$ if $a(\tau)$ changes adiabatically. Because $H \simeq \omega^2 z^2 \simeq P^2$, the amplitude of particle oscillations z and the energy spread of trapped particles $\Delta_{rms}(\tau) = \sqrt{\langle P^2\rangle - \langle P\rangle^2}$ scale with the amplitude $|a(\tau)|$ as

$$z \propto \sqrt{\frac{1}{\omega}} \propto a^{-1/4}, \quad \Delta_{rms}(\tau) \propto \sqrt{\omega} \propto a^{1/4}. \tag{42}$$

Additional to the oscillations, a particle trapped in the micro-potential-well drifts with the potential well at the rate $d\zeta/d\tau = \nu$ as it is clear from Fig. (3). It is easy to see that particle can be trapped as long as $|\zeta| < z_{dr} = a/\Omega^2$.

The condition of adiabaticity which is implied here requires that the shift of a well minimum $\Delta\zeta \simeq \nu\Delta T$ during one period of oscillations of trapped particles $\Delta T = 2\pi/\omega$ is small compared to the well separation 2π. That means $\omega >> \nu$ and is justified for large $a >> \nu^2$.

The time of the drift to the amplitude z_{dr} is $\tau_{dr} = a/(\nu\Omega^2)$ and the energy of a trapped particle increases in the rf potential well to large values $U_{dr} = (a/\Omega)^2$.

The depth of a micro-well $\Delta U_k(\tau) = U(\zeta_k \mp \pi) - U(\zeta_k)$ in which particles were initially trapped at $\zeta_k(0)$, decreases when $\zeta_k(\tau) > |\zeta_k(0)|$ provided $a(\tau)$ grows slower than $z_k(\tau)$ increases. In this case, the micro-well population would be reduced with time releasing particles. The released particles start synchrotron oscillations with large amplitude z_{dr} and momentum $|P| \simeq \Omega z_{dr}$.

This qualitative picture is confirmed by numeric calculations of a trajectory defined by the equations of motion Eq. (36) with fixed $a = 5.0$ and the zero initial conditions. The result and other parameters are shown in Fig. (4).

The released particles may be trapped again mostly due to the radiation damping because the frequency of the synchrotron oscillations and the tune ν are not commensurate. If damping is strong, particles are trapped and released in a pattern similar to relaxation oscillations, see Fig. (5).

3.1 Growth rate in the nonlinear regime for $\tau < \tau_{dr}$

The distances between macro-bunches released from the micro-wells depend on time. Such bunches are not equidistant as in the case of trapped particles. In addition to that, such

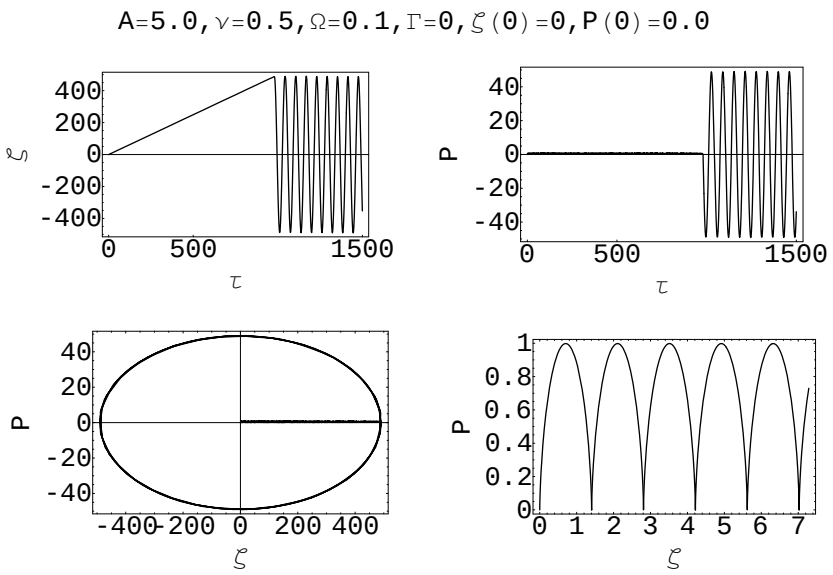

Figure 4: Trajectory of a particle defined by Eq. (36) with a constant amplitude $a = 5.0$. The phase plane is zoomed in the bottom right at small $0 < \tau < 15$ indicating oscillations of trapped and drifting particles. Parameters are shown in the figure. The drift time and the amplitude are in agreement with the estimates $z_{dr} \simeq a/\Omega^2$, $|P| \simeq \Omega z_{dr}$, $\tau_{dr} \simeq z_{dr}/\nu$. At small τ, $\omega \simeq \sqrt{a}$ and the shift in ζ per period is $2\pi\nu/\omega$.

particles have large energy spread and their interaction with the wave is reduced by the Landau damping. Therefore, interaction of such particles with the wave is small. The wave grows mostly due to the interaction with trapped particles what can be approximately described in the following way.

At large amplitudes $a >> \Delta^2$, particles trapped in the micro-wells can be considered as a macroparticle located at the minima ζ_k, see Eq. (39).

Therefore, we can write an approximate expression for the distribution function $F(\zeta, \tau) = \int dP F(\zeta, P, \tau)$ as

$$F(\zeta, \tau) = \sum_k N_k(\tau)\, \delta[\zeta - \zeta_k(\tau)]. \tag{43}$$

Initial micro-bunch population is defined by $F(\zeta, 0) \propto \exp[-(1/2)(\Omega\zeta_k/\Delta)^2]$. There is substantial population

$$N_k(0) = \sqrt{2\pi}(\frac{\Omega}{\Delta})\, e^{-(\frac{\Omega^2}{2\Delta^2})(\frac{2\pi k}{q_0})^2} \tag{44}$$

only in the range $|k| < q_0\Delta/(2\pi\Omega)$, i.e. for $|\zeta_k| < q_0\,(\Delta/\Omega)$. $F(\zeta, \tau)$ is normalized, $\int d\zeta F(\zeta, \tau) = \sum N_k = 1$.

First, we want to show that $F(\zeta, \tau)$ in Eq. (43) during the time less than the drift time τ_{dr} is consistent with the form of the potential U, Eq. (37), provided a and ν are slowly varying with time.

Neglecting slow damping and diffusion, we can replace the Fokker-Plank equation by

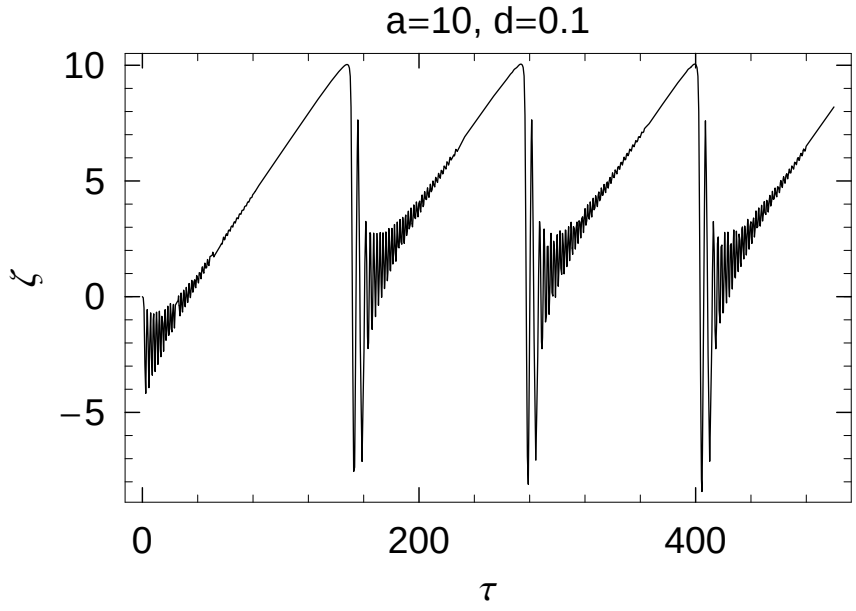

Figure 5: Trajectory of a particle defined by the equation $\zeta'' + \Gamma\zeta' + \zeta = a\sin(\zeta - \nu\tau)$ with the zero initial conditions $z(0) = z'(0) = 0$ in the case of strong damping. Paramaters: $a = 10$, $\Gamma = 0.1$, $\nu = 0.1$

the system of equation of motion Eq. (36) (with $\Gamma = 0$). It is natural to describe the motion of a particle trapped in the k-th micro-well by the coordinates x, $\dot{x}$,

$$x = q_0\zeta - \nu\tau - 2\pi k, \quad \dot{x} = Q = q_0 P - \nu. \tag{45}$$

The oscillations of a particle is defined by the equation

$$\frac{d^2 x_k}{d\tau^2} + \Omega^2 x + a q_0^2 \sin x = -\Omega^2(2\pi k + \nu\tau). \tag{46}$$

For large a, the amplitude of oscillations is small, and $\sin x \simeq x$. Then, Eq. (46) describes a linear oscillator with the frequency ω, $\omega^2 = q_0^2 a + \Omega^2$ and has the solution

$$x(x_0, Q_0, \tau) = -(\frac{\Omega}{\omega})^2(2\pi k + \nu\tau) + [x_0 + 2\pi k(\frac{\Omega}{\omega})^2]\cos(\omega\tau) + \frac{1}{\omega}[Q_0 + \nu(\frac{\Omega}{\omega})^2]\sin(\omega\tau),$$
$$Q(x_0, Q_0, \tau) = -\nu(\frac{\Omega}{\omega})^2 - \omega[x_0 + 2\pi k(\frac{\Omega}{\omega})^2]\sin(\omega\tau) + [Q_0 + \nu(\frac{\Omega^2}{\omega})^2]\cos(\omega\tau). \tag{47}$$

Here, x_0 and Q_0 are constant integrals of motion. They are related to the initial conditions $\zeta(0) = \zeta_0$ and $P(0) = P_0$ at $\tau = 0$,

$$x_0 = q_0\zeta_0 - 2\pi k, \quad Q_0 = q_0 P_0 - \nu. \tag{48}$$

The initial Gaussian bunch $F(\zeta, P, 0) \propto \exp[-\frac{1}{\Delta^2}(P_0^2 + \Omega^2\zeta_0^2)]$. At $\tau > 0$,

$$F(\zeta, P, \tau) = \sum_k \int d\zeta_0 dP_0 F(\zeta_0, P_0, 0)\delta[\zeta - \frac{1}{q_0}(x(\zeta_0, P_0, \tau) + \nu\tau + 2\pi k)]$$
$$\delta[P - \frac{1}{q_0}(Q(\zeta_0, P_0, \tau) + \nu)], \tag{49}$$

where $x(\zeta_0, P_0, \tau)$ and $Q(\zeta_0, P_0, \tau)$ after substitution of x_0 and Q_0 from Eq. (48) are defined by Eq. (47).

Integrating Eq. (49) and averaging terms oscillating with the frequency ω, we get $F(\zeta, P, \tau)$. After additional integration over P,

$$F(\zeta, \tau) = \frac{\Omega}{q_0\Delta^2}\sqrt{\frac{\omega^2 + \Omega^2}{2}} \sum_k e^{-\frac{\omega^2+\Omega^2}{4\Delta^2}[\zeta - \frac{\nu\tau+2\pi k}{q_0(1+\Omega^2/\omega^2)}]^2 - \frac{1}{2}(\frac{2\pi k\Omega}{q_0\Delta})^2}, \tag{50}$$

where small terms of the order of $(\nu/\omega)^2(\Omega/\Delta)^2 << 1$ and $(2\pi k)^2\Omega^4/(\Delta\omega)^2 < (\Omega/\omega)^2 << 1$ are neglected.

Eq. (50) is valid for $(\Omega/\omega)^2|\nu\tau + 2\pi k)| < 1$ that is, for $\tau < \tau_{dr} = \omega^2/(\nu\Omega)$ provided $\omega >> \Omega$.

For large $a >> \Delta^2$, the normalized distribution function Eq. (50) can be written as sum of δ-functions

$$F(\zeta, \tau) = \sum_k \sqrt{2\pi}\,\frac{\Omega}{q_0\Delta}\, e^{-2(\frac{\pi k\Omega}{q_0\Delta})^2}\, \delta[\zeta - \frac{\nu\tau + 2\pi k}{q_0(1 + \Omega^2/\omega^2)}]. \tag{51}$$

This form was assumed in Eq. (43).

The Fourier transform of the distribution function is the sum

$$\tilde{F}(q, \tau) = \sum_k N_k(\tau) e^{-iq\zeta_k(\tau)}. \tag{52}$$

Such a sum is a sharp function of $|q - q_0|$. It can be written as

$$\tilde{F}(q, \tau) = \tilde{F}(q_0, \tau)\Phi(q, q_0, \tau),$$
$$\Phi(q, q_0, \tau) = \frac{\sum N_k(\tau) e^{-iq\zeta_k(\tau)}}{\sum N_k(\tau) e^{-iq_0\zeta_k(\tau)}}. \tag{53}$$

Here

$$\tilde{F}(q_0, \tau) = \int d\zeta\, dP F(\zeta, P, \tau) e^{-iq_0\zeta} \tag{54}$$

and can be easily calculated numerically as it will be shown below.

The factor $\Phi(q, q_0, \tau)$ can be determined using N_k, Eq. (44), and the estimate

$$\sum_{k=-\infty}^{\infty} e^{-2\pi iak - bk^2/2} \simeq \sqrt{\frac{2\pi}{b}}\, e^{-\frac{2\pi^2}{b}\{a\}^2} \tag{55}$$

valid for small $0 < b << 1$. The curly brackets here mean the fractional part of a, $\{a\} = a \bmod(1)$.

Calculations give

$$\Phi(q, q_0, \tau) \propto e^{-\frac{1}{2}(\frac{q_0\Delta}{\Omega})^2\{\frac{q}{q_0(1+\Omega^2/\omega^2}\}^2}. \tag{56}$$

This is a narrow function around q equal to multiples of q_0 with the width $\Delta q = \Omega/\Delta << 1$. The self-consistent potential is generated by the harmonic $q \simeq q_0$. Neglecting all other harmonics, Eq. (56) takes the form

$$\Phi(q, q_0, \tau) = \Phi_0(q - q_0) e^{\frac{q-q_0}{q_0}(1-\frac{\Omega^2}{\omega^2})[-i\nu\tau + (\frac{q_0\Delta}{\omega})^2]}, \tag{57}$$

where

$$\Phi_0(q - q_0) = e^{-\frac{1}{2}(\frac{q_0\Delta}{\Omega})^2(q-q_0)^2}. \tag{58}$$

Numeric calculations of $\Phi(q, q_0, \tau)$ show that the estimate Eq. (57) works very well for the parameters of interest.

Now we can calculate $V(\zeta, \tau) \equiv w(\zeta, \tau) + c.c.$.

The Fourier harmonics $\tilde{w}(q, \tau)$ are defined by Eq. (**??**),

$$\tilde{w}(q, \tau) = -\lambda^3 \int_{-\infty}^{\tau} d\tau' \tilde{F}(q, \tau') e^{i(q-1)\kappa(\tau-\tau')}. \tag{59}$$

Substituting Eqs. (53), (57), we get

$$\tilde{w}(q, \tau) = -\frac{i}{2}\lambda^3 \Phi_0(q - q_0) A(q, q_0, \tau), \tag{60}$$

where

$$A(q, q_0, \tau) = -2i \int_{-\infty}^{\tau} d\tau' \tilde{F}(q_0, \tau') e^{i(q_0-1)\kappa(\tau-\tau')} e^{\frac{q-q_0}{q_0}(1-\frac{\Omega^2}{\omega^2})[-i\nu\tau' + (\frac{q_0\Delta}{\omega})^2]}. \tag{61}$$

Let us consider the short time interval, $\tau < \Delta/(\nu\Omega)$. Then, approximation $\Phi_0(q-q_0) \simeq (2\pi/\lambda^3)\delta(q - q_0)$ gives

$$\begin{aligned} w(\zeta, \tau) &= \int \frac{dq}{2\pi} e^{iq\zeta} \tilde{w}(q, \tau) = -\frac{i}{2} A(q_0, q_0, \tau) e^{iq_0\zeta} \\ A(q_0, q_0, \tau) &= -2i \int_{-\infty}^{\tau} d\tau' \tilde{F}(q_0, \tau') e^{i(q_0-1)\kappa(\tau-\tau')}. \end{aligned} \tag{62}$$

Comparison of the first of Eq.(62) with the assumed form $V(\zeta, \tau) = q_0 a(\tau) \sin(q_0\zeta - \nu\tau)$, defines $a = A(q_0, q_0, \tau)\, e^{i\nu\tau}$.

The largest growth rate can be expected at $q_0 = 1$. To determine the slow dependence on time of the real functions $a(\tau)$ and $\nu(\tau)$ in this case, we use the second of Eq. (62) in the differential form

$$\dot{a} = i\nu a + 2ie^{i\nu\tau}\tilde{F}(q_0,\tau),$$
$$\tilde{F}(q_0,\tau) = \sum_k N_k e^{-iq_0\zeta_k(\tau)} \simeq e^{-i(1-\frac{\Omega^2}{\omega^2})\nu\tau}. \quad (63)$$

Separating real and imaginary parts, we get two equations which can be solved for small $\tau << \tau_{dr}$ where the time of the drift $\tau_{dr} \simeq a/(\nu\Omega^2)$. In this case, the exponent in Eq. (63) can be expanded, giving

$$a(\tau) = [6(\Omega\tau)^2]^{1/3}, \quad \nu = \frac{2}{a}. \quad (64)$$

The amplitude growth depends on Ω and is much faster than that for the coasting beam [1]. The frequency ν decreases with time as $\nu \propto \tau^{-2/3}$.

4 Numerical simulations

In this section, we describe the approximate method based on Eqs. (62) and valid for $\tau < \tau_{dr}$. More general method is described in the next section.

In both cases, we replace the Fokker-Plank equation by the system of equations of motion for each of the n_{part} test particles taking into account the synchrotron motion:

$$\frac{d\zeta}{d\tau} = P,$$
$$\frac{dP}{d\tau} = -\Omega^2\zeta - V(\zeta,\tau) - \Gamma_s P + \xi(\tau). \quad (65)$$

The synchrotron damping and fluctuations are taken into account in the second equation where ξ is random variable,

$$\langle\xi\rangle = 0, \quad \langle\xi(\tau)\xi(\tau')\rangle = 2\Gamma\Delta^2\delta(\tau-\tau'). \quad (66)$$

The interaction $V(\zeta,\tau) = 2\mathrm{Re}[w(\zeta,\tau)]$ for the time intervals $\tau < \tau_{dr}$ can be approximated, see Eqs. (62), as

$$V(\zeta,\tau) = \mathrm{Re}[-iA(\tau)e^{iq_0\zeta}],$$
$$\frac{dA}{d\tau} = i(q_0-1)\kappa A - 2i\tilde{F}(q_0,\tau). \quad (67)$$

Here, $\tilde{F}(q_0,\tau) = \langle e^{-iq_0\tau}\rangle$ can be written in terms of the sum of the n_{part} test particles,

$$\langle e^{-iq_0\zeta}\rangle = \frac{1}{n_{part}}\sum_k e^{-iq_0\zeta_k(\tau)}. \quad (68)$$

Note that we can expect that $A(\tau) \simeq a(\tau)e^{-i\nu\tau}$ where dependence of $a(\tau)$ was estimated in the previous section.

Eqs. (65), (67) and (68) is the full system of equations which were used for simulations.

Initial beam dynamics is the same as one described for the coasting beam [1]. Initial exponential growth predicted by the linear theory is followed at $\tau > 1$ (i.e. $t > \mu$) by oscillations with substantial growth of the rms energy spread.

Results of the long-range tracking of 1000 particles interacting with a single mode $q_0 = 1$ are shown in Figs. (6) and (7). The following parameters were used in the simulation: $\Delta = 0.3$, $\Omega = 0.05$, $\Gamma = 0$. Initially, the amplitude $A(0) = 1.0\,10^{-6}$ and particles were distributed in the phase plane with coordinates $\zeta(0) = \sqrt{2J/\Omega}\sin\theta$, $P(0) = \sqrt{2J\Omega}\cos\theta$ uniformly within the area $-\pi < \theta < \pi$ and $0 < J < \Delta^2/\Omega$.

In Fig. (6) the upper row shows variation in time of the absolute value of the amplitude $|A(\tau)|$ and its real part. The absolute value of the amplitude varies as $|A(\tau)| \propto \tau^\alpha$ where α is between 2/3 and 1. $Re(A)$ oscillates with the frequency ν which decreases while amplitude grows. The second row shows the time dependence of the average and the rms momenta. The increase of the rms momentum follows the estimate Eq. (42). Parameter σ_z depicted in Fig. (6) is the rms length of the of the train of micro-bunches rather than the rms width of the micro-bunch estimated in Eq. (42). The average bunch centroid and bunch length rms are shown in the bottom raw. The distributions over ζ and P are given in the bottom row. Fig. (7) shows the phase plane and the distribution over ζ and momentum at the end of the tracking.

Results confirm the expected drift of particles to large amplitudes and increasing rms momentum spread. The results have to be compared with the estimates Eq. (64) which predict the amplitude $a = 15.5$, the tune $\nu = 2/a$ and the period of oscillations $2\pi/\nu \simeq 90$ at the end of the run (at $\tau = 500$). The growth of the rms momentum follows Eq. (64), and the distance of the drift $z_{dr} = \nu\tau = 64.5$ are in a good agreement with the estimate.

Fig. (8) compares the growth rate of the amplitude for several cases of Δ, Ω and damping Γ. Results confirm that the growth rate depends mostly on Ω and in reasonable agreement with the estimate Eq. (64). The case (a) corresponds to $\Delta = 0.03$, $\Gamma = 0$ and two values of $\Omega = 0.05$ (upper curve) and $\Omega = 0.01$ (lower curve). Eq. (64) predicts in the first/second case $|A| = 15.5$ and $|A| = 5.3$ at $\tau = 500$. In both cases (b) and (c) $\Omega = 0.005$ is the same, but in the case (b) $\Delta = 0.3$ is 10 times larger than in (c) without effect on the growth rate. Effect of the damping is very small and illustrated by the case (d) where damping is turned on, $\Gamma = 0.01$ while $\Delta = 0.03$, and $\Omega = 5E-4$. Such a small Ω does not give any noticeable growth.

The results of numeric simulations discussed above are in good agreement with the analytic estimates of the previous section. It should be reminded, however, that the simulations are based on the equations which are valid only at $\tau < \tau_{dr} \simeq a/[\Omega^2\nu(0)]$ where $\nu(0)$ is the coherent tune shift of the linear approximation.

In the next section we study whether there is an asymptotic steady-state regime.

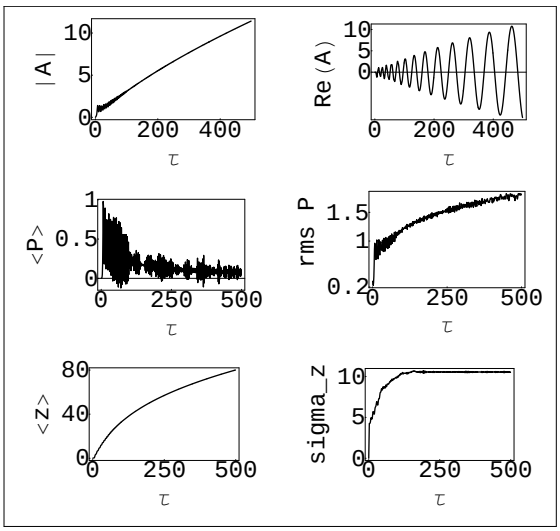

Figure 6: Results of tracking of 1000 particles with zero damping and detuning. Parameters: $A(0) = 1.0E-6$, $\Delta = 0.3$, $\Omega = 0.05$. Upper row: time dependence of $A(\tau)$ (left) and $\mathrm{Re}A(\tau)$ (right). Middle row: variation of the average momentum and the momentum rms with time. Bottom row: time dependence of the bunch centroid and the rms bunch length.

5 Full simulations

For large time intervals $\tau > \tau_{dr}$ most of the initially trapped particles are released and start synchrotron oscillations with large amplitudes. The approximation Eq. (67) can not be used in this case and simulations has to be based on the exact expression Eq. (**??**) for $V(\zeta, \tau)$. Changing variables, we write it as

$$V(\zeta,\tau) = -\frac{\lambda^3}{\kappa}\int_{\zeta}^{\infty} d\zeta' F(\zeta', \tau - \frac{\zeta'-\zeta}{\kappa})\, e^{-i(\zeta-\zeta')} + c.c. \tag{69}$$

In the simulations, we use a mesh covering the range $-20\sigma_\zeta < \zeta < 20\sigma_\zeta$, where $\sigma_\zeta = \Delta/\Omega$ is the initial rms bunch length, divided in bins with the step size $\Delta\zeta$. The later is chosen as $2\pi/12$ to have 12 mesh points within the expected wave length of perturbation $\lambda = 2\pi/q$ with $q = 1$. The total number of mesh points was rounded to $n_m = 512$ to be suitable for Fourier analysis.

Initial distribution of particles in the phase space was the same as in the previous section. To avoid the artificial excitation of bunch centroid motion, the set ζ_k, P_k was corrected to put the average $\langle\zeta\rangle$ and $\langle P\rangle$ to zero.

The time evolution was obtained by solving the equation of motion Eq. (65) with the time steps $\Delta\tau$ for each of the M test particles. The solution on each step was obtained using the subroutine from the FORTRAN IMSL library and the synchrotron radiation diffusion and damping were taken into account at the end of a step by changing variables

p of each particle:

$$p_k \to p_k - \Gamma\Delta\tau p_k + \sqrt{24\Delta\tau\Gamma\Delta^2}\,\xi. \tag{70}$$

Here ξ is random variable uniformly distributed in the interval $-1/2 < \xi < 1/2$ and $k = 1, 2..M$. At each time step, the particle density $F(\zeta)$ was calculated at the mesh points allocating each test particle to the two closest mesh points. Attempt was also made to refine the result changing the width of the bins according to the initial bin population, recalculating the population of the new bins, and recalculating the distribution function. Fig. (9) shows the distribution function calculated with 4, 10, and 20 bins per $\Delta\zeta = 2\pi$ interval. For the following calculations we choose 12 lines per 2π interval as it was mentioned above.

The integral in Eq. (69) was calculated using 3-mesh-point interpolation method. The time step $\Delta\tau = \Delta\zeta/\kappa$ was used to simplify the bookkeeping: with such a choice, the shift by one mesh step $\Delta\zeta$ corresponds also to the shift by one time step $\Delta\tau$. The density $F(\zeta, \tau)$ was stored as a matrix $n_m \times n_m$ and updated at each time step.

Results of simulations depicted below are obtained for the following parameters: $\Delta = 0.3$, $\Omega = 0.05$, $\kappa = 10.0$, $\Gamma = 0.01$. The number of the test particles in simulations was $M = 10^5$. The total number of time steps, 15000, corresponds to the time interval more than 7 damping times. The CPU time for simulations with these parameters is 1.3 hours on 476 MHz PC.

The time evolution of the average momentum and position of the bunch centroid as well as time dependence of the rms of momentum spread and bunch length is shown in Fig. (10).

Distribution of particles in the phase plane (ζ, P) is shown in Fig. (11) at $\tau = 0$ and $\tau = 31.5$, when the instability already substantially distorted the distribution. The snap shots of the phase plane at the end of simulations, $\tau \simeq 700$, are shown in Fig. (12) with the time interval of a quarter of synchrotron period.

The snap shots of the bunch density $F(\zeta, \tau)$ is depicted in Fig. (13) with the time intervals of a quarter of synchrotron period $T_s/4 = 2\pi/(4\Omega)$. The periodic modulation of the density profile is clearly seen in the initial steps of simulations. The amplitude of the modulation decreases with time but does not disappear completely corresponding to the distortion at the periphery of the distribution in the phase plane, see Fig (12). Note also the change of the range in the ζ-axes indicating the synchrotron motion of the bunch centroid.

The first several snap shots of $V(\zeta, \tau)$ vs ζ (left column) and the Fourier spectrum $\tilde{V}(q, \tau)$ vs q (right column) taken with the time interval $\pi/(4\Omega)$. The spectrum is centered at $q \simeq 1$, but become wider with time. The maximum amplitude of $V(\zeta, \tau)$ decreases with time. The time dependence of $V(\tau)$ has some similarity with simulations for continuous spectrum [4] but several peaks in the beginning are transients and disappear later. It is worth noting that these peaks are not artifact or noise: in the interval $0 < \tau < 100$ in Fig. (15) there are 2000 data points.

6 Conclusion

We studied the beam dynamics affected by the microwave coherent synchrotron radiation (CSR) generated by relatively long bunches in storage rings close to the shielding threshold where it can be dominated by a single EM mode excited in the beam pipe. In the dimensionless variables, there are only few parameters Δ, Ω and κ, which determine the instability. For high frequency perturbations, the ratio $\Omega/\Delta << 1$. The linear theory predicts strong instability and generation of the EM wave with the exponentially growing amplitude where the growth rate is larger than the synchrotron frequency. We tried to understand whether such growth may lead to a steady-state saturation regime that would have interesting experimental implications. We show that, in the nonlinear regime, the synchrotron motion substantially affects the instability. After initial exponential growth of the linear regime at the time intervals $\tau <\simeq 1$, the beam dynamics is substantially different for the time intervals small and large than the drift time τ_{dr}. In the first interval, particles are trapped by fast growing wave leading to formation of a chain of micro-bunches. The particle density is strongly modulated with the wave length of the mode. The energy spread of particles is much larger than the initial rms Δ. The interaction of a chain of trapped particles with the wave is strong and the wave amplitude V grows in time faster than for a coasting beam. Later, for $\tau > \tau_{dr}$, most of particles are pulled to the edge of the rf potential, released, and start synchrotron oscillations with large amplitudes. Because trapped particle are released asymmetrically only at one edge of the rf potential well, strong oscillations of the bunch centroid are excited. The released particle do not form a regular pattern in the bunch density. The modulation of the bunch distribution is visible only at the periphery of the phase plane and the amplitude of the generated wave V decreases. The remnant amplitude, nevertheless, is sufficient to compensate the synchrotron radiation damping and support the large energy spread in the bunch. There are several peaks in $V(\tau)$ dependence but they are transient phenomena.

If particles survive, they can be trapped again due to the radiation damping. However, the trapping and the drift of trapped particles both lead to a large rms energy spread and to oscillations of particles with large synchrotron amplitudes. In the beam pipe with a finite aperture that would lead to particle loss and, probably, makes such regime of instability inappropriate for applications. Probably, a betatron with the coasting beam may have advantage compared to the bunched beam in synchrotrons for a machine designed as a source of microwave radiation.

7 Acknowledgement

I thank G. Stupakov, K. Bane for their help and useful discussions.

References

[1] S. Heifets, G. Stupakov, Single mode coherent radiation instability. SLAC-PUB-9627, January 2003.

[2] S. Heifets, G. Stupakov, Beam instability abd microbunching due to coherent synchrotron radiation, PRST, 5, 054402 (2002)

[3] Workshop on Coherent Synchrotron Radiation in Storage Rings, Napa, California, October 28-29, 2002.

[4] M. Venturini and R. Warnock, Bursts of CSR in Electron Storage Rings: a Dynamical Model. Phys.Rev.Lett. 89, 22, 2002.

8 Appendix: interaction of the beam with a single mode

The equation for electric field can be obtained analogously to one given for the coasting beam, see Appendix [1],

$$\mathcal{E}(z,t) = \frac{ie(1-\beta_g)\chi}{\beta_g}\int dz'dt' f(z',t')\int\frac{dq}{(2\pi)}e^{iq[z-z'+c(t-t')]}$$
$$\int\frac{d\omega}{(2\pi)}\frac{e^{-i\omega(t-t')}}{q-q(n,\omega)-i\epsilon}. \tag{71}$$

Integration over ω is defined by the contribution of the pole $\omega_n(q) = q$,

$$\int\frac{d\omega}{2\pi}\frac{e^{-i\omega(t-t')}}{q-q(n,\omega)-i\epsilon} = iv_n(q)\Theta(t-t')e^{-i\omega_n(q)(t-t')}, \tag{72}$$

where $v_n(q) = d\omega_n(q)/dq$, and $\Theta(t-t')$ is the step-function.

The force $\mathcal{E}(z,t) = eE(ct+z,t)$ acting on the trailing particle with displacement z from the bunch centroid ($z > 0$ is in the head of the bunch) is given by the longitudinal component $E(s,t)$ excited by the bunch,

$$\mathcal{E}(z,t) = -e^2c(1-\beta_g)N_b\chi_n\int dt'dz' f(z',t')\Theta[t-t']$$
$$\int\frac{dq}{2\pi}e^{iq(ct+z)-i\omega_n(q)t}e^{-iq(ct'+z')+i\omega_n(q)t'} + c.c. \tag{73}$$

Here $f(z,t)$ is the distribution function of the bunch normalized by the condition $\int dz f(z,t) = 1$, and the coefficient is determined using definition of the loss factor χ_n of the n-th mode for a point-like bunch, $f(z,t) = \delta(z)$. Eq. (73) shows that the sign of $\epsilon > 0$ in Eq. (72) corresponds to the condition of casuality.

Neglecting dispersion $d^2(\omega/c)/dq^2 \simeq b^3/R^2$ (where b is the beam pipe radius and R is the bend radius), we can expand $\omega_n(q) = q_n c + (q - q_n)v_g$. Here v_g and $\omega_n = q_n c$ are the group velocity and frequency of the synchronous component of the n-th mode, respectively. Then

$$\mathcal{E}(z,t) = -e^2 c(1-\beta_g) N_b \chi_n \int_{-\infty}^{t} dt' f[z + c(1-\beta_g)(t-t'), t']\, e^{-iq_n c(1-\beta_g)(t-t')} + c.c. \quad (74)$$

In the steady-state, where $f(z,t) = f(z)$,

$$\mathcal{E} = -e^2 N_b \chi \int_{z}^{\infty} dz' f(z') e^{-iq_n(z'-z)} + c.c. \quad (75)$$

In the dimensionless variables, see Eq. (**??**), the interaction V in Eq. (9) is

$$V = -\frac{dP}{d\tau} = -\frac{\lambda^3}{\kappa} \int_{\zeta}^{\infty} d\zeta' f(\zeta') e^{i(\zeta - \zeta')} + c.c.. \quad (76)$$

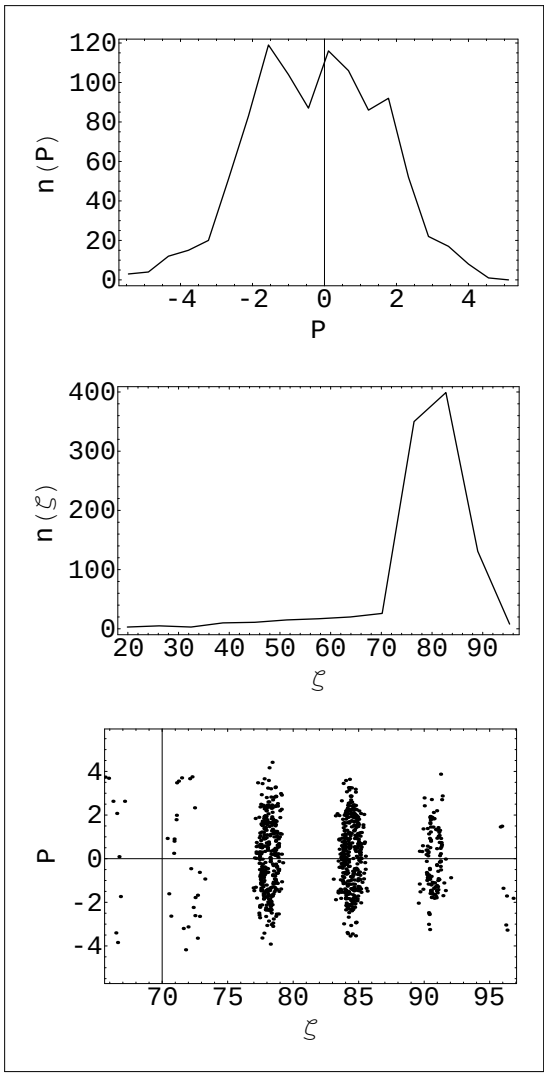

Figure 7: Results of tracking of 1000 particles with zero damping and detuning. Parameters are the same as in Fig. (6). From top to bottom: $n(P)$, $n(\zeta)$, and the phase plane of a bunch, respectively, at the end of tracking, $\tau = 500$.

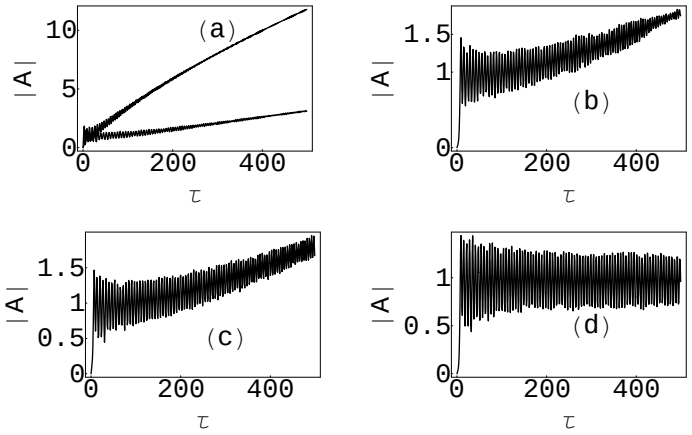

Figure 8: Dependence of the growth rate on parameters. Case (a): $\Delta = 0.03$, $\Gamma = 0$, and $\Omega = 0.05$ (upper curve) and $\Omega = 0.01$ (lower curve). Eq. (64) predicts at $\tau = 500$ $|A| = 15.5$ and $|A| = 5.3$, respectively. Case (b): $\Omega = 0.005$,$\Delta = 0.3$, $\Gamma = 0$. Case (c): $\Omega = 0.005$,$\Delta = 0.03$, $\Gamma = 0$. Case (d) $\Delta = 0.03$, $\Omega = 5E-4$ and damping is on, $\Gamma = 0.01$.

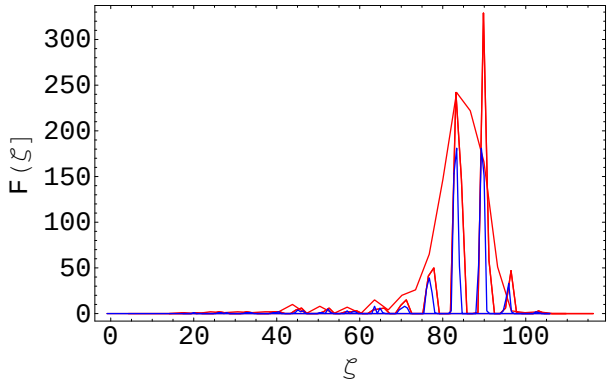

Figure 9: The distribution function calculated with 4, 10, and 20 bins per $\Delta\zeta = 2\pi$ interval.

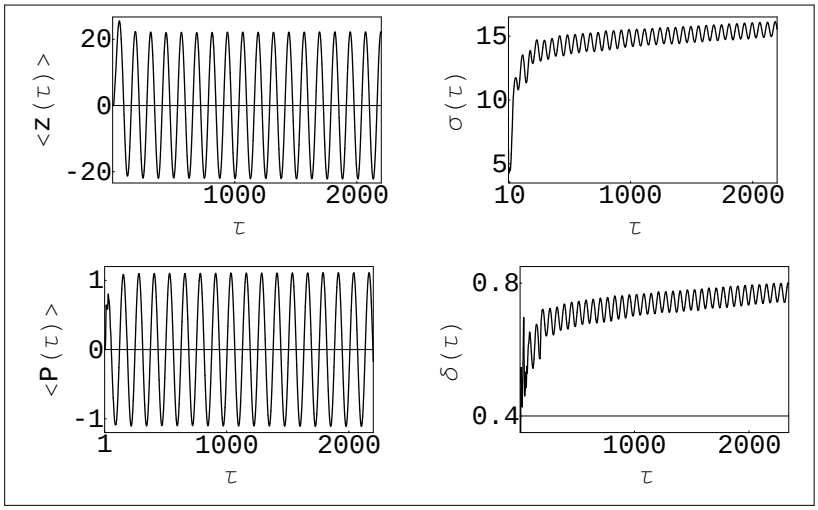

Figure 10: The variation of the average momentum, position of the bunch centroid, the rms energy spread, and the rms bunch length with time. The fast initial growth is replaced by the synchrotron oscillations with large amplitudes.

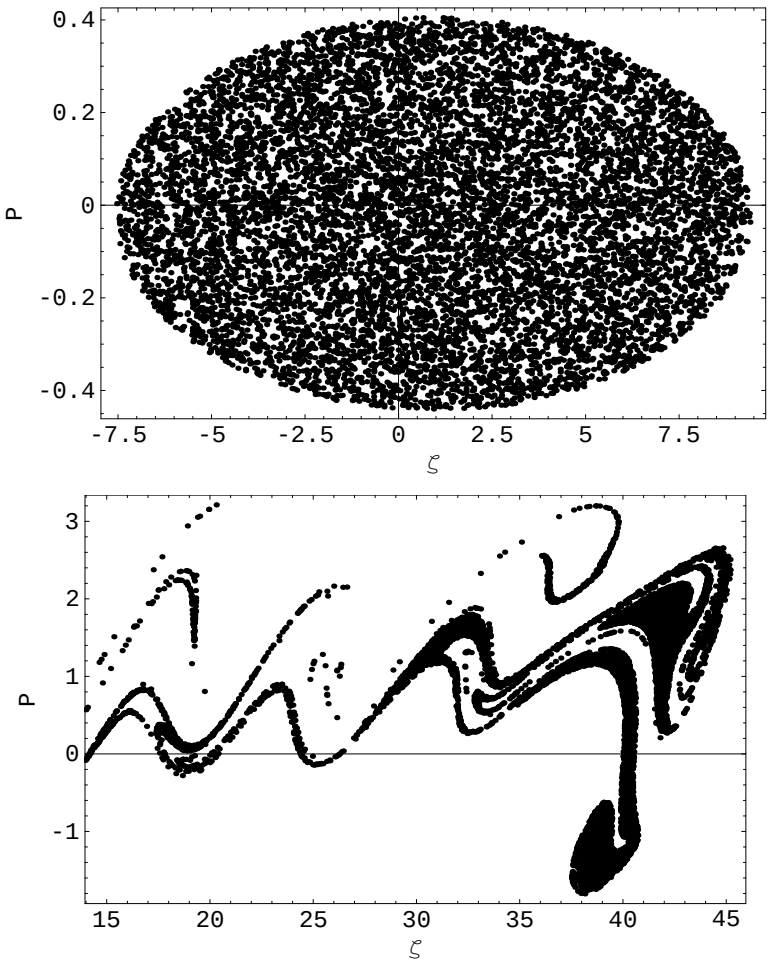

Figure 11: The distribution of particles in the phase plane: initial, $\tau = 0$, (above) and at $\tau = 31.5$.

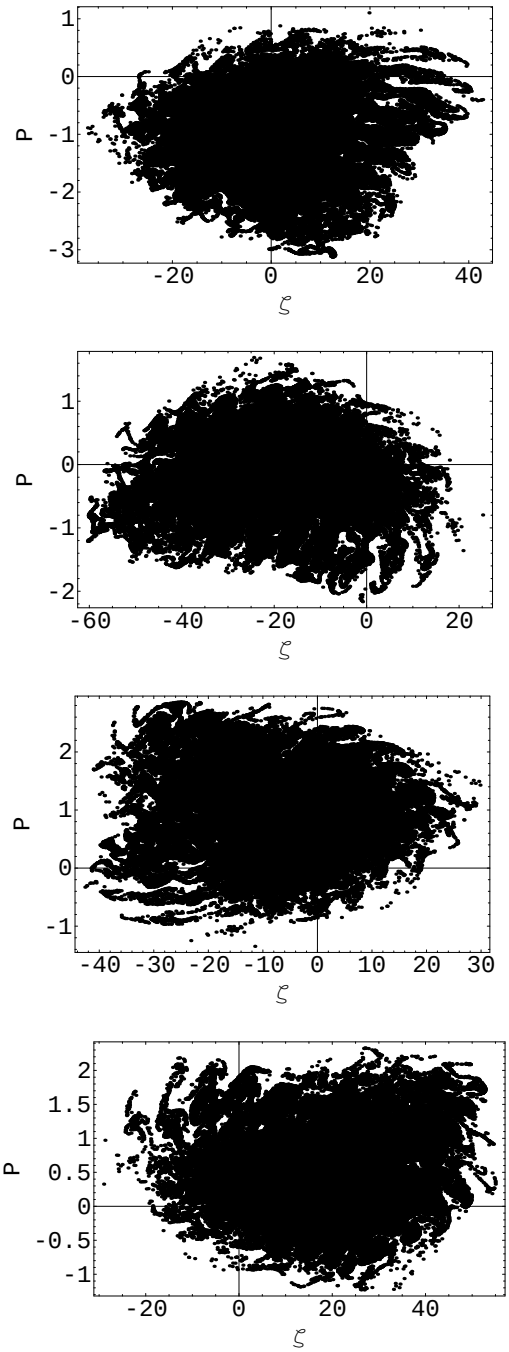

Figure 12: The snap shots of the phase plane at $\tau \simeq 700$ with the time interval $T_s/4$. Note the difference in the position of the bunch centroid.

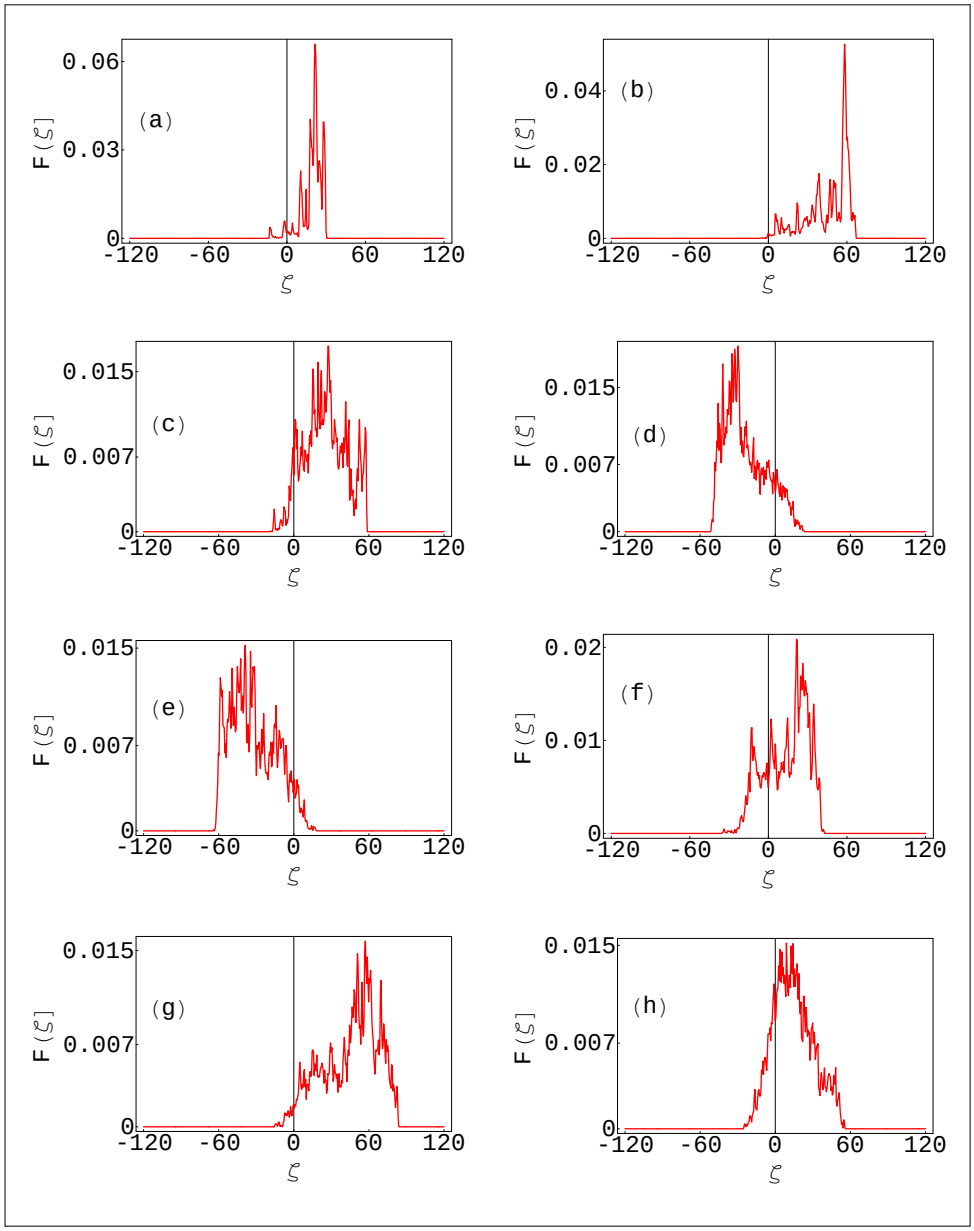

Figure 13: The bunch density $F(\zeta, \tau)$ depicted with the time interval $T_s/8$. Note the difference in the position of the bunch centroid.

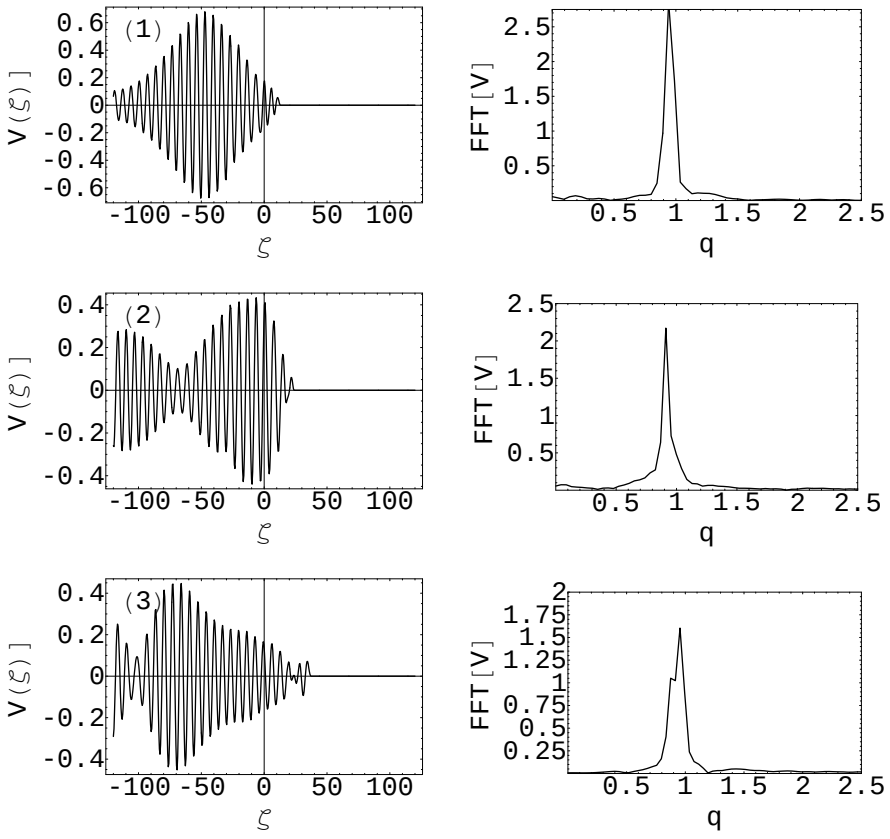

Figure 14: The first several snap shots of $V(\zeta, \tau)$ vs ζ (left column) and the Fourier spectrum $\tilde{V}(q, \tau)$ vs q (right column) taken with the time interval $\pi/(4\Omega)$. The spectrum is centered at $q \simeq 1$, but become wider with time.

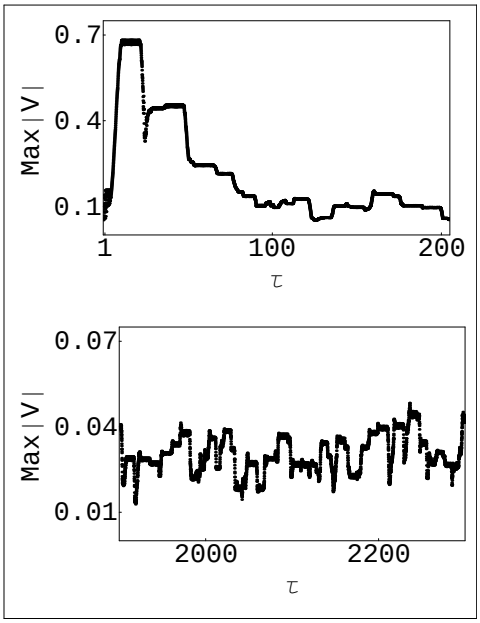

Figure 15: The maximum amplitude of $V(\zeta, \tau)$ vs τ displayed for two time intervals. Data taken at each time step: about 2000 data points in the interval $0 < \tau < 100$. Initially, there are several picks which become smaller later but do not disappear completely.